Effect of Off-Target Binding on ^{18}F-Flortaucipir Variability in Healthy Controls Across the Life Span

Suzanne L. Baker[1], Theresa M. Harrison[2], Anne Maass[2,3], Renaud La Joie[4], and William J. Jagust[1,2]

[1]Lawrence Berkeley National Laboratory, Berkeley, California; [2]Helen Wills Neuroscience Institute, University of California–Berkeley, Berkeley, California; [3]German Center for Neurodegenerative Diseases, Magdeburg, Germany; and [4]Memory and Aging Center, University of California–San Francisco, San Francisco, California

Measuring early tau accumulation is important in studying aging and Alzheimer disease and is only as accurate as the signal-to-noise ratio of the tracer. Along with aggregated tau in the form of neurofibrillary tangles, ^{18}F-flortaucipir has been reported to bind to neuromelanin, monoamine oxidase, calcifications, iron, leptomeningeal melanocytes, and microhemorrages. Although ^{18}F-flortaucipir successfully differentiates healthy controls (HCs) from subjects with Alzheimer disease, variability exists in the cortical signal in amyloid-negative HCs. We aimed to explore the relationship between off-target binding signal and variability in the cortical signal in HCs. **Methods:** Subjects (n = 139) received ^{11}C-Pittsburgh compound B (PIB) and ^{18}F-flortaucipir PET scans and a magnetization-prepared rapid gradient echo MRI scan. PET frames were realigned and coregistered to the MR images, which were segmented using FreeSurfer. In amyloid-negative HCs (n = 90; age range, 21–94 y), 7 nonspecific or off-target binding regions were considered: caudate, pallidum, putamen, thalamus, cerebellar white matter, hemispheric white matter, and choroid plexus. These regions of interest were assigned to 3 similarly behaving groups using principle components analysis, exploratory factor analysis, and Pearson correlations for caudate, putamen, and pallidum (also correlated with age); thalamus and white matter; and choroid plexus. In amyloid-negative HCs with ^{11}C-PIB and ^{18}F-flortaucipir scans, correlations were calculated between white and gray matter before and after partial-volume correction. **Results:** The correlation between white and gray matter disappeared after partial-volume correction in ^{11}C-PIB (r^2 = 0) but persisted for ^{18}F-flortaucipir (r^2 = 0.27), demonstrating that the correlation between white and gray matter signal in ^{18}F-flortaucipir is not solely due to partial-volume effects. A linear regression showed that off-target signal from putamen and thalamus together explained 64% of the variability in the cortical signal in amyloid-negative HCs (not seen in amyloid-positive HCs). Variability in amyloid-negative HCs but not amyloid-positive HCs correlated with white matter signal (unrelated to partial-volume effects) and age-related off-target signal (possibly related to iron load). **Conclusion:** The noise in the ^{18}F-flortaucipir measurement could pose challenges when studying early tau accumulation.

Key Words: tau; ^{18}F-flortaucipir PET; off-target binding

J Nucl Med 2019; 60:1444–1451
DOI: 10.2967/jnumed.118.224113

Accumulation of the tau protein as neurofibrillary tangles and the amyloid-β protein as plaques is the hallmark of Alzheimer disease and also occurs in some healthy controls (HCs). Studying these proteins in vivo is important in understanding aging and Alzheimer disease. The typical pattern of tau deposition in brain aging and dementia has been well established in autopsy studies (*1*). The use of PET with radiopharmaceuticals that bind to tau permits longitudinal in vivo investigations of tau deposition across the life span.

^{18}F-flortaucipir (also known as T807 and ^{18}F-AV-1451) is a PET tracer that binds with high affinity to paired helical filament tau in neurofibrillary tangles (*2,3*). ^{18}F-flortaucipir scans differentiate between HC and Alzheimer disease subjects and parallel Braak stage neurologic tau progression (*4–8*). ^{18}F-flortaucipir scans have shown that tau accumulation is mostly restricted to the medial temporal lobe in HCs (*9*), unless cortical amyloid-β is present, when the tracer is found in isocortical regions (*5–7*). Yet there is wide variability in ^{18}F-flortaucipir SUV ratios (SUVRs) from amyloid-negative HCs ($HC_{A\beta-}$) in regions outside the medial temporal lobes (*10*). Although ^{18}F-flortaucipir demonstrates great promise as a clinical and research tool, off-target binding (OFF), or ^{18}F-flortaucipir signal where aggregated tau is not expected, may complicate image interpretation (*11,12*). We hypothesized that variability in ^{18}F-flortaucipir signal seen in cortical regions outside the medial temporal lobes in $HC_{A\beta-}$ could be related to OFF.

Examples of ^{18}F-flortaucipir OFF include binding in caudate, putamen, pallidum, and thalamus (*4,13*) seen in HCs, where tau accumulation should not occur until late Alzheimer disease stages. These regions also have ^{18}F-flortaucipir tracer kinetics different from the kinetics in cortical regions (*13–16*), further supporting the idea that the ligand binds to targets other than pathologic tau in these regions.

Iron accumulation and age correlate with ^{18}F-flortaucipir in the basal ganglia in HCs (*17*) making iron or ferritin a possible source of ^{18}F-flortaucipir OFF. ^{18}F-flortaucipir also binds to neuromelanin, which increases with age (*18,19*). Neuromelanin plays a role in the sequestration of iron and is found in lower concentrations in the cerebellum than in cortical regions (*20*). Although ^{3}H-flortaucipir binds to monoamine oxidase A (MAO-A) and B (MAO-B) in vitro (*21*), in vivo studies have yet to replicate ^{18}F-flortaucipir binding to MAO-A or MAO-B (*22*). Both exist in lower concentrations in the cerebellum than the cortex (*23*). Also, there was no significant difference in the ^{18}F-flortaucipir OFF in the basal ganglia between Parkinson disease patients receiving MAO-B inhibitors and those who were not (*22*). Many targets have been postulated to explain the binding of ^{18}F-flortaucipir in the choroid

Received Nov. 29, 2018; revision accepted Feb. 20, 2019.
For correspondence or reprints contact: Suzanne L. Baker, Lawrence Berkeley National Laboratory, 1 Cyclotron Rd., MS55R0121, Berkeley, CA 94720.
E-mail: slbaker@lbl.gov
Published online Mar. 15, 2019.

plexus (ChPlex) (*19,24*), although a difference in ^{18}F-flortaucipir-ChPlex between African American and Caucasian subjects suggests ^{18}F-flortaucipir could be binding to neuromelanin (*25*). Lastly, variability in hemispheric white matter (HemiW) signal was reported in HCs as minor displaceable binding (*19*), leading us to classify white matter (WM) as an OFF region.

To summarize, ^{18}F-flortaucipir OFF has been reported in caudate, putamen, pallidum, thalamus, ChPlex, and HemiW. In ^{18}F-flortaucipir imaging in $HC_{A\beta-}$, a range of 0.5 SUVR units has been reported in the cortex (*10*). OFF could account for variability in cortical ^{18}F-flortaucipir in $HC_{A\beta-}$. We explored the relationship between OFF and cortical binding in $HC_{A\beta-}$ and amyloid-positive HCs ($HC_{A\beta+}$) to better understand the variability in the ^{18}F-flortaucipir SUVRs.

MATERIALS AND METHODS

Subjects

HC subjects (n = 139; Table 1) were recruited from the Berkeley Aging Cohort Study for ^{18}F-flortaucipir scans (132 of 139 subjects also had a ^{11}C-Pittsburgh compound B (PIB) scan to determine amyloid status). Berkeley Aging Cohort Study eligibility required that subjects be living independently in the community, perform normally on neuropsychologic examinations, be taking no medications that interfere with cognition, have no medical conditions that affect cognition, and have no contraindications to MRI or PET examinations. The Institutional Review Board of Lawrence Berkeley National Laboratory approved this study; all subjects gave written informed consent.

PET Acquisition

At Lawrence Berkeley National Laboratory, ^{11}C-PIB and ^{18}F-flortaucipir were synthesized at the Biomedical Isotope Facility; subjects were scanned on a Siemens Biograph TruePoint PET/CT. CT was performed at the start of each emission scan for attenuation correction. For ^{11}C-PIB, subjects were injected with 555 MBq at the start of the emission scan. Subjects were scanned for 90 min, and frames were binned as 4 × 15, 8 × 30, 9 × 60, 2 × 180, 10 × 300, and 2 × 600 s. For ^{18}F-flortaucipir, subjects were injected with 370 MBq, and the emission scan was acquired 75–115 min after injection. Data were collected in list mode, allowing 80–100 min to be reconstructed as four 5-min frames. PET data were reconstructed using an ordered-subset expectation maximization algorithm with attenuation and scatter correction and a 4-mm gaussian kernel.

MRI Acquisition

The subjects received a high-resolution T1-weighted magnetization-prepared rapid gradient echo (MPRAGE) scan (repetition time/echo time, 2,110/3.58 ms; flip angle, 15°; 1 × 1 × 1 mm resolution) on a 1.5-T Siemens Magnetom Avanto scanner at Lawrence Berkeley National Laboratory. MRI data were used to define regions of interest (ROIs) for image analysis.

Data Processing

MPRAGE images were segmented using FreeSurfer, version 5.3 (http://surfer.nmr.mgh.harvard.edu/). All coregistration and realignment steps were performed using SPM12 (http://www.fil.ion.ucl.ac.uk/spm/software/spm12/). ^{18}F-flortaucipir individual frames were realigned to create a mean, which was then coregistered to the subject's MPRAGE image.

All ^{18}F-flortaucipir analyses used SUVRs with an inferior cerebellar gray matter reference region (*26*), except for a SUV analysis examining the stability of the cortex, OFF ROIs, and reference region. Data underwent partial-volume correction (PVC) using a geometric transfer matrix approach (*26,27*) using a combination of FreeSurfer ROIs, extracortical hot spots, and SPM12 segmentations for cerebrospinal fluid, skull, and meninges. Both non-PVC and PVC data were analyzed. Mean SUVRs of HemiW, cerebellar WM (CereW), caudate, pallidum, putamen, thalamus, ChPlex, and cortical ROIs (grouped as Braak-stage ROIs (*28*)) and whole cortex (composite of Braak-stage ROIs) were calculated. Braak I was defined as FreeSurfer-segmented entorhinal cortex. II was hippocampus. III was parahippocampal gyrus, fusiform gyrus, amygdala, and lingual gyrus. IV was middle and inferior temporal cortices, temporal pole, insula, and anterior, posterior, and isthmus cingulate gyrus. V was frontal cortex, lateral occipital cortex, parietal cortex, precuneus, banks of superior temporal sulcus, accumbens, and superior and transverse temporal cortices. VI was pericalcarine, precentral, paracentral, and postcentral gyrus, and cuneus.

For ^{11}C-PIB data, the first 5 min of data were summed and subsequent frames were realigned to the first 5 min of data. Data were coregistered to the MPRAGE image. To determine whether subjects were $HC_{A\beta+}$ or $HC_{A\beta-}$, Logan graphical analysis distribution volume ratios (*29*) were calculated (35–90 min; reference region was cerebellar gray matter). The ^{11}C-PIB index was calculated using the weighted mean of FreeSurfer-derived prefrontal, parietal, lateral temporal, and cingulate cortices. HCs without a ^{11}C-PIB scan and under 50 y old or with a ^{11}C-PIB distribution volume ratio of less than 1.065 were considered $HC_{A\beta-}$ (*30,31*).

Statistical Comparisons

Associations Between OFF ROIs and Age in $HC_{A\beta-}$. Pearson correlations (r^2) were calculated on ^{18}F-flortaucipir SUVRs to determine which OFF ROIs were correlated with each other or with age. Age was included in these analyses because possible targets for OFF

TABLE 1
Subjects with No Significant Difference Between $HC_{A\beta-}$ and $HC_{A\beta+}$ in MMSE or Education

Age range (y)	*n*	Sex (M/F)	MMSE	Education (y)	Amyloid group	Has ^{11}C-PIB scan (*n*)
20–35	14	12/2	29 ± 1.2*	15.5 ± 1.4**	Aβ−	9
35–55	5	4/1	29.2 ± 1.8	17.2 ± 1.8	Aβ−	3
55–75	24	10/14	29.0 ± 1.2	17.8 ± 1.7	Aβ−	24
75–95	47	18/29	29.0 ± 1.0	16.9 ± 1.8	Aβ−	47
55–95	49	20/29	28.5 ± 1.4	16.5 ± 1.8	Aβ+	49

*One subject missing MMSE.
**Two subjects missing years of education.
MMSE = Mini-Mental State Examination.

(iron, MAO-B) are correlated with age. OFF ROIs were caudate, pallidum, putamen, thalamus, HemiW, CereW, and ChPlex. The grouping of OFF ROIs was also examined with exploratory factor analysis and principle components analysis. These analyses were done only in the $HC_{A\beta-}$ subjects ($n = 90$; non-PVC and PVC) to minimize the likelihood of on-target binding of ^{18}F-flortaucipir to tau, especially outside the medial temporal lobe. As expected, exploratory factor analysis and principle components analysis confirmed the grouping patterns revealed by Pearson correlations; these ROIs were grouped together for future analyses.

$HC_{A\beta+} > HC_{A\beta-}$. Differences between $HC_{A\beta-}$ (aged 55–95 y) and $HC_{A\beta+}$ for ^{18}F-flortaucipir SUVRs in Braak ROIs and OFF ROIs were tested using analysis of covariance (controlling for age and sex). Partial η^2, the portion of variance accounted for by the amyloid status, was calculated.

Correlations Between Age/OFF ROIs and Braak ROIs. To define the proportion of OFF that might be included in cortical ROIs, Pearson correlations (r^2) were calculated between ^{18}F-flortaucipir SUVRs in individual OFF ROIs (and age) and whole cortex, Braak I, II, III/IV, and V/VI ROIs. This was done separately in $HC_{A\beta-}$ and $HC_{A\beta+}$ groups. Significance of correlations were Bonferroni-corrected for multiple comparisons.

Multiple Linear Models in $HC_{A\beta-}$. Multiple linear models were fit using SUVRs from an ROI from each of the OFF ROI groups to model the variability in the whole-cortex and individual Braak ROIs. This resulted in an adjusted r^2 as well as βs and P values for OFF ROIs for each model. This was done separately in $HC_{A\beta-}$ and $HC_{A\beta+}$ groups.

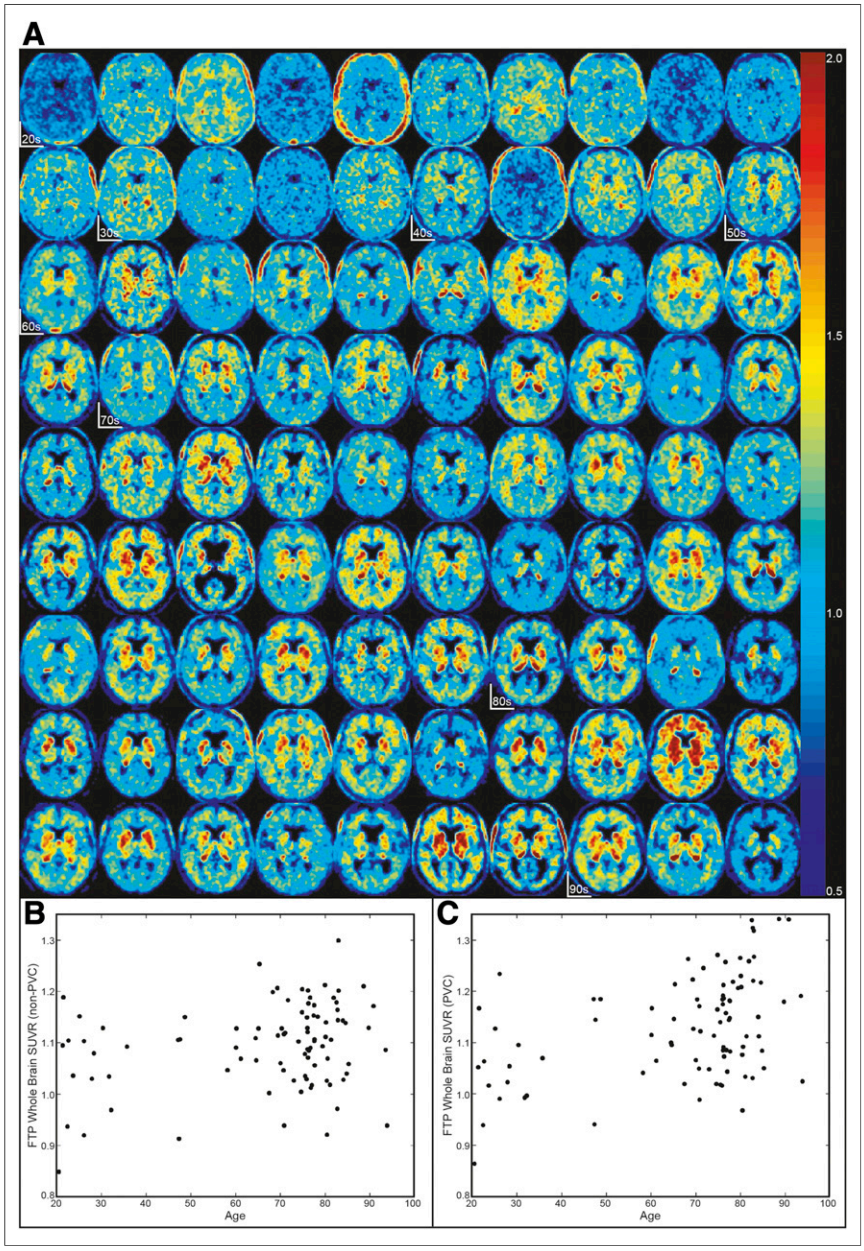

FIGURE 1. High variability in $HC_{A\beta-}$. (A) ^{18}F-flortaucipir SUVR images in Montreal Neurological Institute space in order of age. Start of each age decade is marked. (B) Age vs. non-PVC whole-cortex SUVR ($r^2 = 0.06$, $P < 0.05$). (C) Age vs. PVC whole-cortex SUVR ($r^2 = 0.18$, $P < 0.001$).

Is Cortical Variability Being Driven by Variability in the Reference Region?

Without arterial sampling data, it is difficult to conclude whether the variability in the cortical SUVRs is due to actual cortical variability or to variability in the reference region. To explore this, we calculated the mean, SD, and coefficient of variation of ^{18}F-flortaucipir SUVs in OFF ROIs and Braak-ROIs in $HC_{A\beta-}$.

Is Cortical Variability Being Driven by WM Variability and Partial-Volume Effects (PVEs)?

Because we found that ^{18}F-flortaucipir signal in cortex and HemiW are correlated, we investigated whether this was related to PVE, shared OFF, or both by comparing WM and cortical signal in ^{11}C-PIB and ^{18}F-flortaucipir SUVR images before and after PVC in the same subjects ($HC_{A\beta-}$ subjects; $n = 83$). Since PVEs should be similar for ^{11}C-PIB and ^{18}F-flortaucipir, comparison of the effect of PVC for these 2 tracers should provide some evidence for how much of the binding is related to PVE and how much is related to shared binding to targets.

For this comparison, ^{11}C-PIB scans were processed using an approach similar to the one applied to the ^{18}F-flortaucipir data. ^{11}C-PIB SUVRs were calculated from 50 to 70 min, the data underwent PVC using the same set of ROIs as for ^{18}F-flortaucipir, and inferior cerebellar gray matter was the reference region. Means of HemiW, CereW, and cortex were calculated with and without PVC. Pearson correlations were calculated between cortical tracer binding and HemiW and CereW for ^{18}F-flortaucipir and ^{11}C-PIB SUVRs (non-PVC and PVC).

RESULTS

High Variability of ^{18}F-Flortaucipir Retention in $HC_{A\beta-}$

Figure 1 demonstrates the variability seen across $HC_{A\beta-}$ subjects. Even in subjects younger than 40 y, who should have

TABLE 2
Positive Correlations Between Age and OFF ROIs

Parameter	Caudate	Pallidum	Putamen	Thalamus	HemiW	CereW	ChPlex
Age							
Non-PVC data	0.42*	0.64*	0.68*	0.30*	0.13	0.15**	0.03
PVC data	0.57*	0.55*	0.71*	0.12	0.00	0.01	0.12
Caudate							
Non-PVC data		0.72*	0.77*	0.67*	0.58*	0.55*	0.11
PVC data		0.59*	0.83*	0.41*	0.13	0.18*	0.08
Pallidum							
Non-PVC data			0.92*	0.69*	0.55*	0.56*	0.07
PVC data			0.66*	0.40*	0.21*	0.25*	0.10
Putamen							
Non-PVC data				0.68*	0.52*	0.51*	0.06
PVC data				0.38*	0.10	0.13	0.08
Thalamus							
Non-PVC data					0.79*	0.79*	0.21*
PVC data					0.61*	0.66*	0.02
HemiW							
Non-PVC data						0.83*	0.11
PVC data						0.83*	0.01
CereW							
Non-PVC data							0.09
PVC data							0.02

*$P < 0.001$, corrected for multiple comparisons.
**$P < 0.01$, corrected for multiple comparisons.

no global cortical tau accumulation (*32*), the whole cortical SUVR shows considerable variability, ranging from 0.85 to 1.19 (non-PVC) and 0.86 to 1.23 (PVC).

Associations Between OFF ROIs and with Age in $HC_{A\beta-}$

Pearson intercorrelations between all OFF ROI SUVRs and between each OFF ROI and age in all $HC_{A\beta-}$ subjects are shown for both non-PVC and PVC (Table 2) data. Age and ^{18}F-flortaucipir binding in caudate, pallidum, and putamen are highly correlated with one another (non-PVC, $r^2 > 0.4$; PVC, $r^2 > 0.5$) and were also grouped into one factor (exploratory factor analysis) and component (principle components analysis) (Supplemental Tables 1–2; supplemental materials are available at http://jnm.snmjournals.org). SUVR in thalamus is weakly correlated with caudate, putamen, and pallidum but more strongly correlated with HemiW and CereW. Thalamus and WM were also grouped together using exploratory factor analysis and principle components analysis. The higher correlations seen in HemiW with caudate, pallidum, and putamen for non-PVC data are most likely due to PVEs, demonstrated by lower r^2 for PVC correlations. Lastly, ^{18}F-flortaucipir binding in ChPlex significantly correlated with thalamus before PVC and with nothing after PVC. Results from Pearson correlations, principle components analysis, and exploratory factor analysis support the 3 different groups of OFF ROIs: age, caudate, pallidum, and putamen (the age-related group); thalamus, HemiW, and CereW; and ChPlex.

$HC_{A\beta+} > HC_{A\beta-}$

Figure 2 shows the comparison between $HC_{A\beta-}$ and $HC_{A\beta+}$ for Braak and OFF ROIs. There was no significant difference in ^{18}F-flortaucipir SUVR OFF ROIs between $HC_{A\beta+}$ and $HC_{A\beta-}$ when controlling for age and sex (non-PVC and PVC; amyloid status partial $\eta^2 \leq 0.06$). There was a significant difference in ^{18}F-flortaucipir SUVR for all Braak ROIs between $HC_{A\beta+}$ and $HC_{A\beta-}$ subjects.

Age/OFF-to-Braak ROIs

We next investigated relationships between age, OFF ROIs, and cortical ^{18}F-flortaucipir binding by performing Pearson correlations for non-PVC (Figs. 3A and 3B) and PVC SUVRs (Figs. 3C and 3D) in $HC_{A\beta-}$ (Figs. 3A and 3C) and $HC_{A\beta+}$ (Figs. 3B and 3D). Within $HC_{A\beta-}$ subjects, correlations of cortical binding with OFF ROIs decrease after PVC but remain significant, demonstrating that PVEs alone cannot explain the correlations. All correlations in $HC_{A\beta+}$ are lower than in $HC_{A\beta-}$ subjects. In $HC_{A\beta+}$, Braak II (hippocampus) has the highest correlations with OFF ROIs; however, none are significant after PVC. Predictably, in $HC_{A\beta+}$, HemiW has significant correlations with Braak II–VI before PVC, but nothing is significant after PVC.

Multiple Linear Models

Whole cortex showed the strongest correlations after PVC with putamen (from the age-related OFF ROIs) and thalamus (from the WM and thalamus OFF ROIs). Therefore, we used putamen,

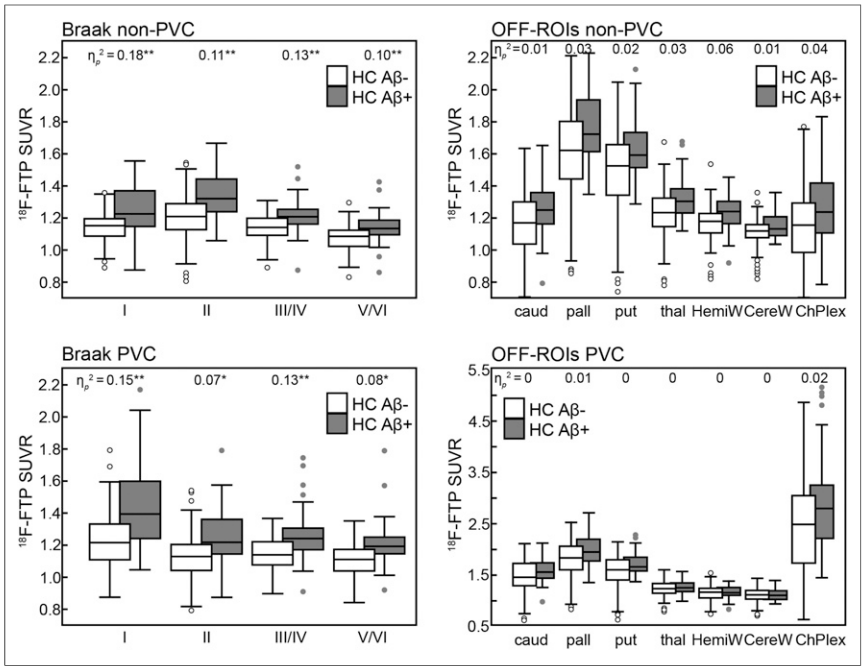

FIGURE 2. Comparison between $HC_{A\beta-}$ and $HC_{A\beta+}$ in Braak and OFF ROIs with and without PVC. Central mark indicates median. Top and bottom of box indicate 75th and 25th percentiles, respectively. Whisker extent indicates median ± 1.57(75th percentile − 25th percentile)/square root(number subjects). C represents subjects beyond whisker extent. Significance of $P < 0.005$ (*) and $P < 0.001$ (**) denoted for η_p^2.

thalamus, and ChPlex as independent measures and whole cortex and Braak ROIs as dependent measures with a series of multiple linear models to explore how well OFF accounted for cortical variability in $HC_{A\beta-}$ subjects. The βs and adjusted r^2 are reported in Table 3 for Braak I, II, III/IV, V/VI, and whole cortex. The βs are the weights for putamen, thalamus, and ChPlex in the linear model resulting in the r^2, with the Braak ROI or whole cortex as the dependent variable. For example, the linear equation for PVC whole cortex is (0.1 × putamen) + (0.33 × thalamus) + (0.01 × ChPlex). To put the βs into perspective, the mean SUVR in $HC_{A\beta-}$ subjects for putamen was 1.47 ± 0.29 (non-PVC) and 1.54 ± 0.35 (PVC), thalamus was 1.24 ± 0.18 (non-PVC and PVC), and ChPlex was 1.15 ± 0.22 (non-PVC) and 2.78 ± 0.94 (PVC). A lower amount of variability was explained in Braak I (adjusted $r^2 = 0.30$ and 0.22 for non-PVC and PVC) than in other Braak regions. ChPlex was only significant when explaining variability in the signal for the hippocampus (Braak II). Thalamus was significant ($P < 0.01$) in explaining SUVR for all Braak ROIs. Putamen was significant ($P < 0.001$) in explaining Braak III/IV, V/VI, and whole cortex (PVC), and Braak II (non-PVC, $P < 0.01$).

Multiple linear models were also performed in $HC_{A\beta+}$ (data not shown). Only the linear model for Braak II resulted in a significant ($P < 0.001$) adjusted r^2 (non-PVC = 0.59, PVC = 0.31); thalamus and ChPlex significantly contributed to the model.

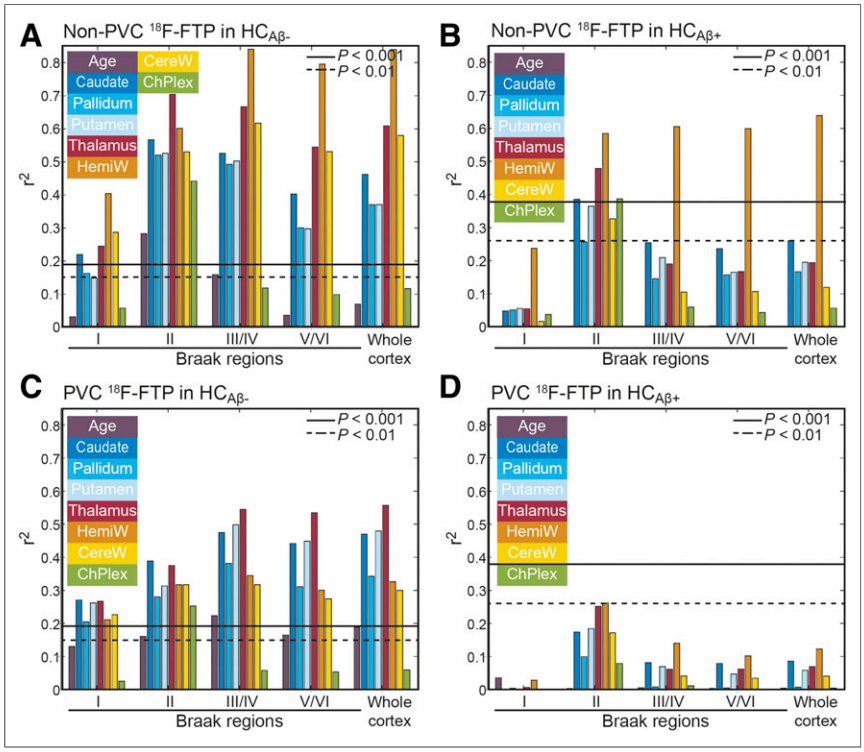

FIGURE 3. Pearson r^2 between ^{18}F-flortaucipir SUVR in cortical regions, age, and OFF ROIs. *P* values were Bonferroni-corrected.

Is Cortical Variability Being Driven by Variability in the Reference Region?

Whether the cortical variability was driven by reference region in ^{18}F-flortaucipir was explored by calculating the coefficient of variation of SUVs in $HC_{A\beta-}$ subjects, shown in Supplemental Table 3. Coefficient of variation was similar across regions but was smallest in the inferior cerebellar gray matter; the mean and SD of SUV were smallest in the inferior cerebellar gray matter, leading us to believe that inferior cerebellar gray matter is a sufficient reference region and is not the cause of the cortical variability.

Is Cortical Variability Being Driven by WM Variability and PVEs?

The PVEs of WM on cortical gray matter were explored by comparing the correlation between WM (HemiW and CereW) and cortical gray matter in ^{18}F-flortaucipir SUVR before and after PVC. We decided to examine both HemiW and CereW because CereW does not suffer from PVEs from whole cortex. To gauge the degree of correlation expected from PVEs, the analysis was also done in

TABLE 3
Series of Multiple Linear Models (Run in $HC_{A\beta-}$) with Flortaucipir SUVRs in Cortical ROIs as Dependent Measure and SUVRs in Putamen, Thalamus, and ChPlex as Independent Measures

Dependent variable	Independent-variable β			Adjusted r^2
	Putamen	Thalamus	ChPlex	
Braak I non-PVC	−0.02	0.34*	0	0.22**
Braak I PVC	0.16	0.38*	0.01	0.30**
Braak II non-PVC	0.14*	0.39**	0.26**	0.82**
Braak II PVC	0.07	0.42**	0.07**	0.55**
Braak III/IV non-PVC	0.03	0.38**	−0.01	0.66**
Braak III/IV PVC	0.11**	0.31**	0.01	0.64**
Braak V/VI non-PVC	−0.07	0.49**	−0.03	0.55**
Braak V/VI PVC	0.09**	0.33**	0.01	0.61**
Whole-cortex non-PVC	−0.04	0.46**	−0.02	0.60**
Whole-cortex PVC	0.10**	0.33**	0.01	0.64**

*$P < 0.01$.
**$P < 0.001$.

^{11}C-PIB SUVRs in the same subjects. The analysis was limited to $HC_{A\beta-}$ subjects to minimize any on-target binding. Figure 4 shows the corresponding HemiW versus mean of whole cortex for the 83 subjects. ^{11}C-PIB correlations between HemiW and whole cortex changed from 0.19 to 0 as a result of PVC (CereW correlations with cortex also went from 0.19 to 0), demonstrating that PVC can remove the correlation between white and gray matter signal. However, PVC did not remove the correlations between white and gray matter signal in ^{18}F-flortaucipir; HemiW to whole cortex was $r^2 = 0.84$ for non-PVC and decreased to 0.27 as a result of PVC (^{18}F-flortaucipir CereW to whole cortex went from $r^2 = 0.57$ to 0.23 after PVC). All correlations between gray and white matter were significant at $P < 0.001$ except for PVC ^{11}C-PIB.

DISCUSSION

^{18}F-flortaucipir is a useful tracer to examine pathologic tau load differences between HCs and subjects with Alzheimer disease. However, in $HC_{A\beta-}$, where tau paired helical filaments are unlikely to be found in substantial numbers in the neocortex (*33,34*), there is a variability in cortical signal (*10*) that makes measuring early tau deposition challenging. We showed that 64% of the cortical signal variability in our $HC_{A\beta-}$ subjects can be explained by signal from OFF ROIs (Table 3). Furthermore, the mean cortical ^{18}F-flortaucipir variability in $HC_{A\beta-}$ subjects has an SUVR range of 0.5 SUVR units and is similar in $HC_{A\beta-}$ subjects younger than 40 y old (these subjects have a low likelihood of having neocortical tau (*33,34*)). Similar variability in $HC_{A\beta-}$ ^{18}F-flortaucipir cortical signal was also shown in 422 $HC_{A\beta-}$ subjects (*10*).

There is a possibility that there is little variability in Braak ROI SUVRs in $HC_{A\beta-}$ subjects and that the variability seen stems from the reference region. In an attempt to determine whether variability in the reference region could be driving this, we calculated SUVs for $HC_{A\beta-}$. The reference region, inferior cerebellar gray matter, had the lowest coefficient of variation of SUVs of all the ROIs. The inferior cerebellar gray matter is no more or less stable than other regions. It has been shown that the cerebellum has a similar distribution volume (calculated using arterial sampling data) between HCs and subjects with Alzheimer disease (*16*), implying a certain level of stability. However, it has also been shown that the distribution volume calculated from arterial input function correlates with age (with different slopes) both in the cerebellum and in cortical regions (*15*).

The 3 OFF ROI groups were an age-related group (which included caudate, pallidum, and putamen), a WM group (which included thalamus), and ChPlex. The age-related group could be driven by binding to neuromelanin or iron. Iron load (quantified using MRI R_2*) has been shown to correlate with ^{18}F-flortaucipir binding in the basal ganglia and age in HCs and Alzheimer disease patients (*17*); additionally, in HCs, pallidum and putamen have been reported to have higher iron than other ROIs, which we also observed for ^{18}F-flortaucipir in our $HC_{A\beta-}$ cohort. The age-related OFF contribution to variability in cortical signal is relatively small.

The WM group of OFF ROIs contributed more to the variability in the cortical signal than the age-related group in a multiple linear regression. Correlations between CereW and Braak ROIs were similar to correlations between HemiW and Braak ROIs after PVC. CereW and Braak ROIs are not proximal and therefore do not contribute to each other's PVEs, implying that the correlations between WM and Braak ROIs are not driven solely by PVEs. We further explored the possibility that PVEs drive the cortical signal variability in ^{18}F-flortaucipir by looking at the relationship between WM and whole cortex in ^{18}F-flortaucipir and ^{11}C-PIB scans before and after identical PVC approaches. We showed that ^{11}C-PIB WM signal could be removed from cortical signal using PVC, but a correlation between WM and cortical signal persisted after PVC in ^{18}F-flortaucipir scans. This suggests that the correlation between the WM and gray matter signal is a real feature of ^{18}F-flortaucipir binding properties and not the result of PVEs. WM explains substantial variance of signal in the cortex of the $HC_{A\beta-}$. It is unclear what ^{18}F-flortaucipir could be binding to in WM, although the lipophilic nature of β-sheet binding tracers may explain this finding.

ChPlex did not significantly correlate with any OFF ROI or age, except thalamus before PVC (not significant after PVC). ChPlex significantly correlated only with hippocampus non-PVC SUVR in $HC_{A\beta-}$ and $HC_{A\beta+}$ and PVC SUVR in $HC_{A\beta-}$ and significantly contributed only to the multiple linear model predicting hippocampal SUVR. Although ChPlex makes quantification of hippocampus SUVR challenging, the OFF in this region does not correlate with other OFF ROIs or Braak regions outside the hippocampus. Along with being steeped in PVEs, the hippocampus is also known to have automated segmentation problems (*8*). Segmentation inaccuracies would negatively impact the precision of non-PVC and PVC quantification. Hippocampus ^{18}F-flortaucipir signal should be interpreted with caution.

PVEs are not the only source of the variability in ^{18}F-flortaucipir signal in $HC_{A\beta-}$, nor did our PVC algorithm create correlations where none existed. The correlations between cortex and WM existed in both non-PVC and PVC data, and most correlations between cortical and OFF ROIs decreased as a result of PVC. The agreement between non-PVC and PVC results leads us to conclude that the OFF in the cortical regions is not an artifact of data analysis.

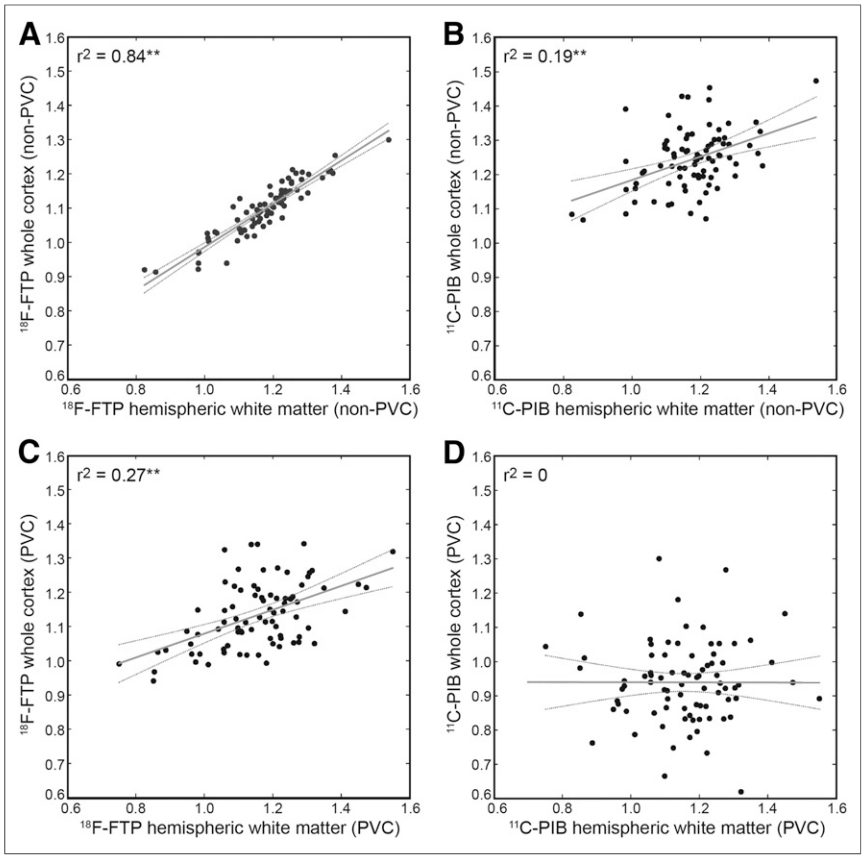

FIGURE 4. Correlations between HemiW and whole-cortex SUVRs: non-PVC ^{18}F-flortaucipir (A), non-PVC ^{11}C-PIB (B), PVC ^{18}F-flortaucipir (C), and PVC ^{11}C-PIB (D). Gray line = linear model fit; dashed gray lines = 95% confidence interval. $^{**}P < 0.001$.

Focusing on only the $HC_{A\beta-}$ subjects, OFF ROIs account for less of the signal variance in Braak I (entorhinal cortex) than other Braak regions. Because entorhinal cortex is the site of earliest accumulation of tau in HCs, this is most likely due to true binding of ^{18}F-flortaucipir to tau in subjects in this region. In contrast, more than 50% of cortical signal variability could be explained by OFF ROIs in $HC_{A\beta-}$ subjects.

In $HC_{A\beta+}$ subjects, OFF ROIs were only significant predictors of hippocampal ^{18}F-flortaucipir signal. There is a significant difference between $HC_{A\beta+}$ and $HC_{A\beta-}$ subjects' Braak ROI SUVRs but no significant difference in OFF ROI SUVRs. When OFF ROIs were correlated to Braak ROIs in $HC_{A\beta+}$ subjects, there were few significant correlations in the non-PVC data (save hippocampus, HemiW, and caudate) and no significant correlations after PVC. These 2 results lead us to conclude that ^{18}F-flortaucipir is binding to tau in $HC_{A\beta+}$ subjects. The ratio of on-target binding to OFF in $HC_{A\beta+}$ subjects seems to be high enough that the OFF ROI correlations are not significant. However, an interesting future direction would be to quantify the relative amounts of on-target binding and OFF in $HC_{A\beta+}$ subjects.

It is beyond the scope of this paper to analyze the variability of the OFF ROI and Braak signal within subjects, longitudinally. It has been shown that the use of HemiW as a reference region for longitudinal tau data reduced variability and enhanced discrimination between diagnostic cohorts (*35*). The success of the HemiW reference region could be partly related to covariance of HemiW and gray matter, and therefore normalizing by HemiW would remove that white-matter–related OFF signal from the gray matter.

CONCLUSION

Although ^{18}F-flortaucipir has been shown to track tau deposition in the brain, OFF increases variability in the cortical signal in $HC_{A\beta-}$ subjects. There are 3 main ROI groups with related OFF signal: an age-related group including the caudate, pallidum, and putamen; a WM-related group including the thalamus; and lastly the ChPlex. This variability is correlated to a signal likely related to iron deposition, as well as the amount of ^{18}F-flortaucipir measured in the WM. PVEs do not completely account for the variability in the cortical signal. The variability in signal in HCs related to OFF should be considered when studying the earliest deposition of tau using ^{18}F-flortaucipir. Either the sample size should be sufficient to account for the variability across subjects, or possibly, controlling for measurements of OFF when correlating ^{18}F-flortaucipir measurements with other neuroimaging or cognitive measure could result in improved sensitivity.

DISCLOSURE

This research was supported by NIH grant AG034570. Suzanne Baker serves as a consultant to Genentech. William Jagust serves as a consultant to Bioclinica, Genentech, Novartis, and Biogen. No other potential conflict of interest relevant to this article was reported.

KEY POINTS

QUESTION: Is the variability in cortical binding of flortaucipir related to off-target binding in PET scans in amyloid-negative healthy controls?

PERTINENT FINDINGS: Sixty-four percent of the variability in the flortaucipir cortical signal in subjects with little to no tau can be explained by off-target signal in the putamen (age-related) and in the thalamus (lipophilicity-related). These correlations are no longer significant in subjects with cortical tau accumulation.

IMPLICATIONS FOR PATIENT CARE: Measuring the earliest deposition of tau using flortaucipir may be challenging due to cortical signal variability in amyloid-negative healthy controls.

REFERENCES

1. Braak H, Braak E. Neuropathological stageing of Alzheimer-related changes. *Acta Neuropathol (Berl).* 1991;82:239–259.
2. Chien DT, Bahri S, Szardenings AK, et al. Early clinical PET imaging results with the novel PHF-tau radioligand [F-18]-T807. *J Alzheimers Dis.* 2013;34:457–468.
3. Xia CF, Arteaga J, Chen G, et al. [^{18}F]T807, a novel tau positron emission tomography imaging agent for Alzheimer's disease. *Alzheimers Dement.* 2013;9:666–676.
4. Johnson KA, Schultz A, Betensky RA, et al. Tau positron emission tomographic imaging in aging and early Alzheimer disease. *Ann Neurol.* 2016;79:110–119.

5. Schöll M, Lockhart SN, Schonhaut DR, et al. PET imaging of tau deposition in the aging human brain. *Neuron.* 2016;89:971–982.
6. Schwarz AJ, Yu P, Miller BB, et al. Regional profiles of the candidate tau PET ligand ^{18}F-AV-1451 recapitulate key features of Braak histopathological stages. *Brain.* 2016;139:1539–1550.
7. Wang L, Benzinger TL, Su Y, et al. Evaluation of tau imaging in staging Alzheimer disease and revealing interactions between beta-amyloid and tauopathy. *JAMA Neurol.* 2016;73:1070–1077.
8. Ossenkoppele R, Rabinovici G, Smith R. Discriminative accuracy of [^{18}F]flortaucipir positron emission tomography for Alzheimer disease vs other neurodegenerative disorders. *JAMA.* 2018;320:1151–1162.
9. Schultz SA, Gordon BA, Mishra S, et al. Widespread distribution of tauopathy in preclinical Alzheimer's disease. *Neurobiol Aging.* 2018;72:177–185.
10. Lowe VJ, Wiste HJ, Senjem ML, et al. Widespread brain tau and its association with ageing, Braak stage and Alzheimer's dementia. *Brain.* 2018;141:271–287.
11. Sander K, Lashley T, Gami P, et al. Characterization of tau positron emission tomography tracer [^{18}F]AV-1451 binding to postmortem tissue in Alzheimer's disease, primary tauopathies, and other dementias. *Alzheimers Dement.* 2016;12: 1116–1124.
12. Barrio JR. The irony of PET tau probe specificity. *J Nucl Med.* 2018;59:115–116.
13. Baker SL, Lockhart SN, Price JC, et al. Reference tissue-based kinetic evaluation of ^{18}F-AV-1451 for tau imaging. *J Nucl Med.* 2017;58:332–338.
14. Shcherbinin S, Schwarz AJ, Joshi A, et al. Kinetics of the tau PET tracer ^{18}F-AV-1451 (T807) in subjects with normal cognitive function, mild cognitive impairment, and Alzheimer disease. *J Nucl Med.* 2016;57:1535–1542.
15. Barret O, Alagille D, Sanabria S, et al. Kinetic modeling of the tau PET tracer ^{18}F-AV-1451 in human healthy volunteers and Alzheimer disease subjects. *J Nucl Med.* 2017;58:1124–1131.
16. Golla SSV, Timmers T, Ossenkoppele R, et al. Quantification of tau load using [^{18}F]AV1451 PET. *Mol Imaging Biol.* 2017;19:963–971.
17. Choi JY, Cho H, Ahn SJ, et al. Off-target ^{18}F-AV-1451 binding in the basal ganglia correlates with age-related iron accumulation. *J Nucl Med.* 2018;59:117–120.
18. Marquié M, Normandin MD, Vanderburg CR, et al. Validating novel tau positron emission tomography tracer [F-18]-AV-1451 (T807) on postmortem brain tissue. *Ann Neurol.* 2015;78:787–800.
19. Lowe VJ, Curran G, Fang P, et al. An autoradiographic evaluation of AV-1451 tau PET in dementia. *Acta Neuropathol Commun.* 2016;4:58.
20. Zecca L, Bellei C, Costi P, et al. New melanic pigments in the human brain that accumulate in aging and block environmental toxic metals. *Proc Natl Acad Sci USA.* 2008;105:17567–17572.
21. Vermeiren C, Motte P, Viot D, et al. The tau positron-emission tomography tracer AV-1451 binds with similar affinities to tau fibrils and monoamine oxidases. *Mov Disord.* 2018;33:273–281.
22. Hansen AK, Brooks DJ, Borghammer P. MAO-B inhibitors do not block in vivo flortaucipir([^{18}F]-AV-1451) binding. *Mol Imaging Biol.* 2018;20:356–360.
23. Tong J, Meyer JH, Furukawa Y, et al. Distribution of monoamine oxidase proteins in human brain: implications for brain imaging studies. *J Cereb Blood Flow Metab.* 2013;33:863–871.
24. Marquie M, Verwer EE, Meltzer AC, et al. Lessons learned about [F-18]-AV-1451 off-target binding from an autopsy-confirmed Parkinson's case. *Acta Neuropathol Commun.* 2017;5:75.
25. Lee CM, Jacobs HIL, Marquie M, et al. ^{18}F-flortaucipir binding in choroid plexus: related to race and hippocampus signal. *J Alzheimers Dis.* 2018;62:1691–1702.
26. Baker SL, Maass A, Jagust WJ. Considerations and code for partial volume correcting [^{18}F]-AV-1451 tau PET data. *Data Brief.* 2017;15:648–657.
27. Rousset OGMY, Evans AC. Correction for partial volume effects in PET: principle and validation. *J Nucl Med.* 1998;39:904–911.
28. Maass A, Landau S, Baker SL, et al. Comparison of multiple tau-PET measures as biomarkers in aging and Alzheimer's disease. *Neuroimage.* 2017;157:448–463.
29. Logan J, Volkow ND, Wang GK, Ding YS, Alexoff DL. Distribution volume ratios without blood sampling from graphical analysis of PET data. *J Cereb Blood Flow Metab.* 1996;16:834–840.
30. Mormino EC, Brandel MG, Madison CM, et al. Not quite PIB-positive, not quite PIB-negative: slight PIB elevations in elderly normal control subjects are biologically relevant. *Neuroimage.* 2012;59:1152–1160.
31. Villeneuve S, Rabinovici GD, Cohn-Sheehy BI, et al. Existing Pittsburgh compound-B positron emission tomography thresholds are too high: statistical and pathological evaluation. *Brain.* 2015;138:2020–2033.
32. van Bergen JMG, Li X, Quevenco FC, et al. Low cortical iron and high entorhinal cortex volume promote cognitive functioning in the oldest-old. *Neurobiol Aging.* 2018;64:68–75.
33. Braak H, Thal DR, Ghebremedhin E, Del Tredici K. Stages of the pathologic process in Alzheimer disease: age categories from 1 to 100 years. *J Neuropathol Exp Neurol.* 2011;70:960–969.
34. Braak H, Braak E. Frequency of stages of Alzheimer-related lesions in different age categories. *Neurobiol Aging.* 1997;18:351–357.
35. Southekal S, Devous MD Sr, Kennedy I, et al. ^{18}F-flortaucipir quantitation using a parametric estimate of reference signal intensity (PERSI). *J Nucl Med.* 2018; 59:944–951.